Exploiting the Abrupt 4 × CO_2 Scenario to Elucidate Tropical Expansion Mechanisms

REI CHEMKE

Department of Applied Physics and Applied Mathematics, Columbia University, New York, New York

LORENZO M. POLVANI

Department of Earth and Environmental Sciences, and Lamont-Doherty Earth Observatory, Columbia University, Palisades, New York

(Manuscript received 29 May 2018, in final form 27 November 2018)

ABSTRACT

Future emissions of greenhouse gases into the atmosphere are projected to result in significant circulation changes. One of the most important changes is the widening of the tropical belt, which has great societal impacts. Several mechanisms (changes in surface temperature, eddy phase speed, tropopause height, and static stability) have been proposed to explain this widening. However, the coupling between these mechanisms has precluded elucidating their relative importance. Here, the abrupt quadrupled-CO_2 simulations of phase 5 of the Coupled Model Intercomparison Project (CMIP5) are used to examine the proposed mechanisms. The different time responses of the different mechanisms allow us to disentangle and evaluate them. As suggested by earlier studies, the Hadley cell edge is found to be linked to changes in subtropical baroclinicity. In particular, its poleward shift is accompanied by an increase in subtropical static stability (i.e., a decrease in temperature lapse rate) with increased CO_2 concentrations. These subtropical changes also affect the eddy momentum flux, which shifts poleward together with the Hadley cell edge. Transient changes in tropopause height, eddy phase speed, and surface temperature, however, were found *not* to accompany the poleward shift of the Hadley cell edge. The widening of the Hadley cell, together with the increase in moisture content, accounts for most of the expansion of the dry zone. Eddy moisture fluxes, on the other hand, are found to play a minor role in the expansion of the dry zone.

1. Introduction

The thermal structure of the atmosphere, and its circulation, are projected to change over the next few decades (IPCC 2013; Vallis et al. 2015). One of the most robust signals to emerge from climate models is the poleward shift of the latitudinal edges of the tropical belt (e.g., Hu et al. 2013; Kang et al. 2013). Such a widening of the tropical belt would directly affect the hydrological cycle in semiarid regions (IPCC 2014), as it pushes the dry zone (where most of the world's deserts are concentrated) poleward, further drying the subtropics (e.g., Lu et al. 2007; Scheff and Frierson 2012).

In spite of the robust tropical expansion projected by climate models, large uncertainty remains in the observed trends over the last several decades (Davis and Rosenlof 2012; Allen et al. 2014; Lucas et al. 2014). Studies have reported that the tropical belt has been expanding poleward at a rate of 0.3°–2° decade^{-1} (Fu et al. 2006; Hudson et al. 2006; Hu and Fu 2007; Archer and Caldeira 2008; Seidel et al. 2008; Nguyen et al. 2013; D'Agostino and Lionello 2017). The wide range of observed trends is mostly due to the wide range of metrics used to define the tropical belt (e.g., tropopause height, subtropical jet, streamfunction, precipitation and evaporation, and outgoing longwave radiation). Furthermore, except for changes in mean meridional mass streamfunction, all other metrics were found to produce trends that are statistically insignificant (Davis and Rosenlof 2012). More recently, it has been shown that many of the metrics that were originally used do not correlate with the streamfunction expansion (Solomon et al. 2016; Davis and Birner 2017) and hence are not representative of a widening Hadley cell.

Corresponding author: Rei Chemke, rc3101@columbia.edu

DOI: 10.1175/JCLI-D-18-0330.1

One of the main difficulties in observing a significant trend is the presence of both the internal variability of the climate system (e.g., Pacific decadal oscillation), which obscures the ongoing anthropogenic forced signal (Allen et al. 2014; Quan et al. 2014; Lucas and Nguyen 2015; Allen and Kovilakam 2017; Mantsis et al. 2017), and the multiplicity of forcing agents (Allen et al. 2012, 2014; Waugh et al. 2015) that are able to affect the width of the tropical circulation. For example, while enhanced greenhouse gas emissions were found to expand the tropical circulation in recent decades (e.g., Bony et al. 2013; Hu et al. 2013), the buildup of anthropogenic aerosols in the Northern Hemisphere were found to contract the circulation, and thus offset the expansion signal (Allen and Ajoku 2016). In the Southern Hemisphere, ozone depletion was found to be the main forcing of tropical expansion in the second half of the twentieth century (Son et al. 2009; Polvani et al. 2011b), and the ongoing recovery of ozone hole will therefore cancel the effect of greenhouse gases throughout the first half of the twenty-first century (Polvani et al. 2011a; Barnes et al. 2014).

The unabated emissions of greenhouse gases into the atmosphere is one of the main contributors to the Hadley cell expansion over the twenty-first century. Therefore, it is important to understand what controls tropical expansion under increased CO_2 concentrations. To avoid complications from the presence of other forcings, we will here confine our attention to the $4 \times CO_2$ scenario, which produces a large tropical expansion with unambiguous attribution. Furthermore, because the quadrupling of CO_2 is instantaneous, it conveniently separates different components of the climate system, which respond with different time scales: this scenario, therefore, allows us to learn a great deal regarding the mechanism of tropical expansion.

Over the last decades, several mechanisms have been proposed to explain the tropical expansion, which we now briefly review. Enhanced CO_2 concentrations warm both the troposphere and sea surface, while cooling the stratosphere. While several studies have claimed that changes in surface temperature T_s are mostly responsible for widening the tropical belt (e.g., Frierson et al. 2007; Adam et al. 2014; Son et al. 2018), others have argued that it is the atmospheric warming that matters the most (e.g., Lu et al. 2009; Bony et al. 2013). Part of this confusion stems from the fact that different time periods were chosen in different studies, as well as the different ozone forcings (Waugh et al. 2015).

Other studies (e.g., Lu et al. 2008; Ceppi and Hartmann 2013) have suggested that changes in eddy phase speed may drive the expansion of the Hadley cell under global warming. The rise of the tropopause height in warmer climates (Thuburn and Craig 1997; Santer et al. 2003) may affect the meridional temperature gradient aloft (Lorenz and DeWeaver 2007), and thus the eddy phase speed (Wittman et al. 2007). Because the mean zonal winds decrease from the midlatitudes equatorward, higher eddy phase speeds may push the subtropical critical latitude poleward (Chen and Held 2007). The dissipation of eddies at critical latitudes implies a poleward shift of the latitude of zero eddy momentum flux divergence. Since the latter balances the mean flow in steady state (e.g., Vallis 2006), this would push the latitudinal extent of the Hadley cell poleward.

While the above studies have proposed possible mechanisms, none of them constitutes an actual theory for why the tropics are expanding with increased CO_2 concentrations. To date, there have been two main theories that provide scalings for the Hadley cell width. The first, proposed by Held and Hou (1980), posits that the Hadley cell is a thermally closed circulation, and that poleward moving air at its upper branch conserves angular momentum. In this theory, the Hadley cell width (ϕ_{HH}) scales as follows:

$$\phi_{\mathrm{HH}} \propto \left(\frac{g H_t \Delta_h \theta}{\Omega^2 a^2 \theta_0} \right)^{1/2}, \tag{1}$$

where g is gravity, Ω is Earth's rotation rate, a is Earth's radius, θ_0 is a reference potential temperature, $\Delta_h \theta$ is the equator-to-pole potential temperature difference in radiative equilibrium, and H_t is the tropical tropopause height.

The second theory, proposed by Held (2000), posits that the Hadley cell edge corresponds to the latitude where the vertical shear of the angular momentum–conserving flow becomes baroclinically unstable, using the two-layer model criterion of Phillips (1954). In this theory the Hadley cell width (ϕ_{H00}) scales as follows:

$$\phi_{\mathrm{H00}} \propto \left(\frac{N H_e}{\Omega a} \right)^{1/2}, \tag{2}$$

where $N^2 = (g/\theta)(\partial\theta/\partial z)$ is the subtropical static stability and H_e is the subtropical tropopause height.

Using idealized GCMs (e.g., Walker and Schneider 2006; Frierson et al. 2007; Levine and Schneider 2015), full atmospheric-only GCMs (e.g., Frierson et al. 2007), and coupled GCMs (e.g., Lu et al. 2007, 2008), it has been shown that, under global warming, the latitudinal extent of the Hadley cell follows the Held (2000) scaling. The tropical expansion was found to correlate with both the increase in subtropical static stability (e.g., Lu et al. 2008; Son et al. 2018) and the subtropical tropopause height, which pushes the baroclinic zone poleward (e.g., Lu et al. 2007).

In all above studies, the long-term response of the tropical expansion was studied (e.g., under statistically steady-state or slowly varying forcing) by correlating it with the above suggested components (e.g., T_s, tropopause height, static stability, and eddy phase speed). Since correlation alone need not imply a casual relation, especially in a highly coupled system, the relative importance of the different components that may drive the widening of the tropical belt could not be estimated.

Studying the evolution of the atmospheric circulation to abrupt change in CO_2, on the other hand, will allow us to elucidate the relative importance of the different components in affecting the steady-state response. For instance, Wu et al. (2012) showed that under abrupt double CO_2 forcing the stratosphere is first to respond, leading to changes in tropospheric eddies that alter the zonal mean circulation. While eddies were found to play an important role in these simulations, changes in eddy phase speed were found not to correlate with circulation changes (Wu et al. 2013; Staten et al. 2014). Using abrupt $4 \times CO_2$ forcing in CMIP5 models, Grise and Polvani (2017) showed that while the Hadley cell expands and reaches 90% of its final location after the first few years, global-mean T_s monotonically increases reaching 90% of its final value only after several decades, implying that global-mean T_s is not the main driver of the Hadley cell expansion.

While the Hadley cell edge and global-mean T_s show different response times to quadrupling CO_2, the poleward expansion of the dry zone (the latitude where precipitation equal evaporation) was found to follow the slower changes in global-mean T_s, rather than the rapid changes in the Hadley cell width (Grise and Polvani 2017). This implies that in spite of the high correlation between the edge of the Hadley cell (streamfunction expansion) and the edge of the dry zone (Quan et al. 2014; Solomon et al. 2016), different mechanisms control them. At steady state, changes in precipitation and evaporation are in balance with moisture flux divergence changes. Both long-term (Seager et al. 2010) and transient (Grise and Polvani 2017) responses point to the importance of the time-mean circulation and transient eddies in shifting the edge of the dry zone poleward. However, the effects of stationary eddy moisture flux, as well as the zonal mean flow, remain unclear.

Here, following Grise and Polvani (2017), the evolution of the Hadley cell expansion, the dry zone's edge, and the above suggested mechanisms, are examined under abrupt $4 \times CO_2$ forcing in CMIP5 models. The different time scales of the response of the relevant components will allow us to determine the relative importance of the different proposed mechanisms in widening the tropics. Since the steady-state result in these simulations stems from the transient response to the abrupt $4 \times CO_2$ forcing, studying the transient response is a key for understanding the equilibrium widening of the Hadley. Because all mechanisms discussed above assume zonal symmetry, and because most of the continents reside in the Northern Hemisphere, the tropical response 0ptto increased CO_2 is here studied only in the Southern Hemisphere, which provides the most appropriate conditions for validating the proposed mechanisms.

The paper is structured as follows. Section 2 describes the different simulations used to study the widening of the tropics, and the different metrics in question. The roles of the different atmospheric components and the two scaling theories on the Hadley cell expansion are examined in sections 3 and 4, respectively. The analysis of the mechanism behind the poleward shift of the dry zone edge is conducted in section 5. Finally, section 6 summarizes the results.

2. Methods

To study the evolution of the different components that affect the Hadley cell width, and the edge of the dry zone, three sets of the "r1i1p1" experiments from the CMIP5 multimodel ensemble (Taylor et al. 2012) are analyzed: first, 200 years of preindustrial control run with a constant 1850 forcing; second, 150 years of abrupt (set as initial conditions) $4 \times CO_2$ forcing (relative to preindustrial values); and third, 140 years of $1\%\,\mathrm{yr}^{-1}$ increased CO_2 run (starting from preindustrial values). For each experiment we analyze 23 coupled models, which are listed in Table 1.

Two key metrics are used for estimating the width of the tropical belt, and are illustrated in Figs. 1a and 1b, respectively, from the preindustrial control run of the GFDL-ESM2G (Dunne et al. 2012):

(i) The edge of the Hadley cell $\phi_{\Psi 500}$ is calculated as the latitude where the meridional mass streamfunction (colors in Fig. 1) Ψ, defined by

$$\Psi = \frac{2\pi a \cos\phi}{g} \int_0^p [\overline{v}]\, dp\,,$$

first changes sign poleward of its maximum value at 500 hPa (green cross in Fig. 1a); ϕ is latitude, p is pressure, v is the meridional velocity, the overbar represents the annual mean, and the square brackets represent the zonal mean.

(ii) The edge of the dry zone ϕ_{P-E} (black cross in Fig. 1b) is evaluated as the latitude where zonal- and annual-mean precipitation P; (red line in Fig. 1b) equals evaporation E (blue line in Fig. 1b) poleward of the latitude of maximum Ψ.

TABLE 1. List of the 23 CMIP5 models, and their atmospheric resolutions, analyzed in this study.

Model	Modeling center	Atmospheric resolution (lon × lat)
ACCESS1.0	Commonwealth Scientific and Industrial Research Organization (CSIRO) and Bureau of Meteorology (BOM), Australia	1.875° × 1.25°
BCC-CSM1.1	Beijing Climate Center, China Meteorological Administration	2.8125° × 2.8125°
BCC-CSM1.1-m	Beijing Climate Center, China Meteorological Administration	1.125° × 1.1°
CanESM2	Canadian Centre for Climate Modeling and Analysis	2.8125° × 2.76°
CCSM4	National Center for Atmospheric Research	1.25° × 0.9°
CNRM-CM5	Centre National de Recherches Meteorologiques	1.4° × 1.39°
CSIRO-Mk3.6.0	Commonwealth Scientific and Industrial Research Organization in collaboration with Queensland Climate Change Centre of Excellence	1.875° × 1.85°
FGOALS-g2	LASG, Institute of Atmospheric Physics, Chinese Academy of Sciences and CESS, Tsinghua University	2.8125° × 1.65°
FGOALS-s2	LASG, Institute of Atmospheric Physics, Chinese Academy of Sciences	2.8125° × 2.8°
GFDL CM3	NOAA Geophysical Fluid Dynamics Laboratory	2.5° × 2°
GFDL-ESM2G	NOAA Geophysical Fluid Dynamics Laboratory	2.5° × 1.5°
GFDL-ESM2M	NOAA Geophysical Fluid Dynamics Laboratory	2.5° × 1.5°
GISS-E2-H	NASA Goddard Institute for Space Studies	2.5° × 2°
GISS-E2-R	NASA Goddard Institute for Space Studies	2.5° × 2°
HadGEM2-ES	Met Office Hadley Centre	1.875° × 1.25°
INMCM4	Institute for Numerical Mathematics	2° × 1.5°
IPSL-CM5B-LR	Institut Pierre-Simon Laplace	3.75° × 1.9°
MIROC-ESM	Japan Agency for Marine-Earth Science and Technology, Atmosphere and Ocean Research Institute (The University of Tokyo), and National Institute for Environmental Studies	2.8125° × 2.76°
MIROC5	Atmosphere and Ocean Research Institute (The University of Tokyo), National Institute for Environmental Studies, and Japan Agency for Marine-Earth Science and Technology	1.4° × 1.39°
MPI-ESM-LR	Max Planck Institute for Meteorology	1.875° × 1.85°
MPI-ESM-P	Max Planck Institute for Meteorology	1.875° × 1.85°
MRI-CGCM3	Meteorological Research Institute	1.125° × 1.1°
NorESM1-M	Norwegian Climate Centre	2.5° × 1.9°

The above metrics are calculated after a 0.1° latitudinal cubic interpolation (which preserves the metrics' latitudinal structure) of Ψ and $P - E$.

In addition, to properly analyze the different mechanisms of tropical expansion discussed in section 1, two other quantities, related to eddy components, are calculated as follows:

(i) The latitude of maximum eddy momentum flux $\phi_{[\overline{u^+v^+}]}$ (orange cross in Fig. 1a), where u is zonal wind, and crosses represent deviation from both zonal and monthly means.
(ii) The phase speed of maximum eddy momentum flux c_{phase} (black cross in Fig. 1c). The eddy momentum flux phase speed is calculated following Randel and Held (1991) at 250 hPa, in segments of consecutive 60 days averaged over each year.

The above eddy quantities are calculated after a 0.1° latitudinal quadratic interpolation (to capture the maximum value of eddy momentum fluxes). Only four models in Table 1 (GFDL-ESM2G, GFDL-ESM2M, MIROC5, and IPSL-CM5B-LR) have available daily data, which are required for calculating eddy fluxes. Thus, the eddy analysis in this study is performed for only these four models.

Finally, ϕ_{HH} and ϕ_{H00} are computed as follows:

(i) The different components in Eq. (1) [the Held and Hou (1980) scaling] are defined as follows; θ_0 as the Southern Hemisphere tropospheric-mean (at 500 hPa) potential temperature, $\Delta_h\theta$ as the equator-to-pole tropospheric-mean potential temperature difference (the difference between the tropical average, 0°S–20°S, and the high-latitude average, 75°–90°S) and the tropical tropopause height H_t as the lowest level where the vertical temperature gradient crosses the $2\,\text{K km}^{-1}$ value, in accordance with the World Meteorological Organization (WMO).
(ii) The different components in Eq. (2) [the Held (2000) scaling] are defined as follows: The subtropical static stability N^2 is averaged between 400–850 hPa, and the subtropical tropopause height H_e follows the above WMO definition. Vertically averaging the static stability up to a constant level, and not up to

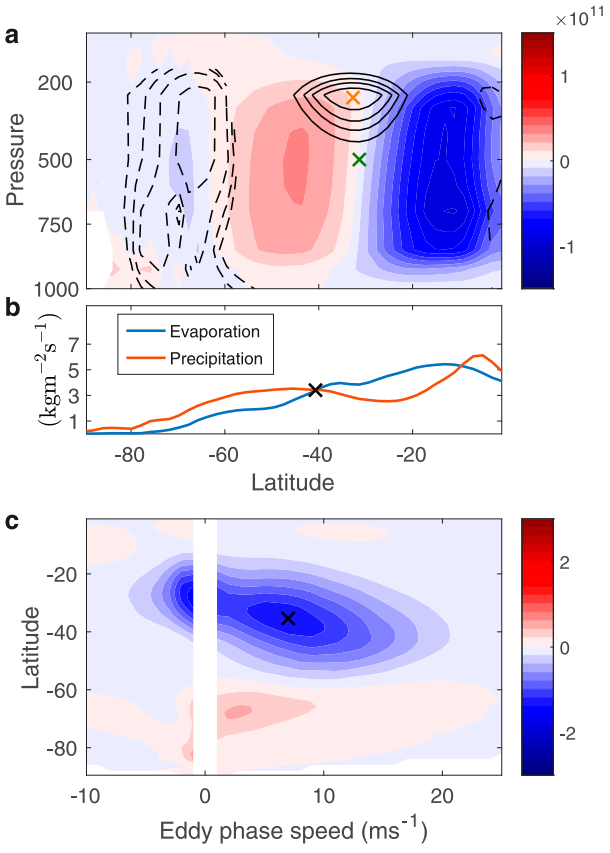

FIG. 1. Metrics for evaluating tropical expansion. (a) Zonal- and time-mean meridional mass streamfunction ($\mathrm{kg\,s^{-1}}$; colors) and eddy momentum flux ($\overline{[u^+v^+]}\cos\phi; \mathrm{m^2\,s^{-2}}$; black contours) as a function of pressure and latitude. The green and orange crosses respectively represent the latitude where the meridional mass streamfunction first changes sign poleward of its maximum value at 500 hPa $\phi_{\Psi 500}$ and the latitude of maximum eddy momentum flux $\phi_{\overline{[u^+v^+]}}$. The eddy momentum flux contours correspond to $[-39, -34, -30, -25, 0.5, 1, 2, 4]\,\mathrm{m^2\,s^{-2}}$. (b) The black cross represents the latitude where precipitation equals evaporation ($10^{-5}\,\mathrm{kg\,m^{-2}\,s^{-1}}$) poleward of the maximum value of the streamfunction ϕ_{P-E}. (c) Eddy momentum flux at 250 hPa as a function of latitude and phase speed ($\mathrm{m^2\,s^{-2}}\,\Delta c^{-1}$). The black cross in (c) represents the phase speed of maximum eddy momentum flux c_{phase}. All panels are based on the preindustrial control run of the GFDL-ESM2G.

the tropopause height, allows disentangling the changes in both of these metrics, as discussed below.

The multimodel mean of each of the above quantities is calculated by first taking its annual and zonal average for each model separately, and then averaging across all models. All subtropical quantities are calculated between 35° and 45°S, and tropical quantities between 0° and 20°S. The subtropical latitudes are defined outside of the Hadley cell in order to properly examine the Held (2000) scaling, which includes extratropical quantitates.

To estimate the response time of each of the above metrics and components to the abrupt 4 × CO_2 forcing, we fit the following function, $y = c_o(1 - e^{-t/\tau})$, to their time evolution, where the parameters c_o and τ are numerically obtained using a least squares algorithm. The response time is then defined by calculating the three e-folding time (3τ). The later provides an estimate of the time when the response of each component reaches ~95% of its steady-state value. Statistically steady-state values are defined as the average over the last 50 years of the 150-yr-long 4 × CO_2 simulations.

3. Assessing the importance of surface temperature and eddy phase speed

As discussed in section 1, two atmospheric components have been proposed to exert a strong influence on the widening of the Hadley cell: 1) the surface temperature T_s and 2) the eddy phase speed c_{phase}. To examine each of these components, their evolution, under the abrupt 4 × CO_2 forcing, is examined and compared to the poleward shift of $\phi_{\Psi 500}$.

a. *Surface temperature changes*

Several previous studies argued for the importance of T_s in affecting the Hadley cell width. Both the global-mean T_s (e.g., Staten et al. 2012; Quan et al. 2014; Son et al. 2018) and the meridional T_s gradient (e.g., Frierson et al. 2007; Adam et al. 2014) have been suggested to affect the Hadley cell width. However, as these suggestions are based on correlations in the long-term response across many models, no causality arguments can be made. To examine whether changes in T_s vary together with the widening of the Hadley circulation, the evolutions of $\phi_{\Psi 500}$ (black), the Southern Hemisphere mean T_s (blue), and the meridional T_s gradient ($\Delta_h T_s$; purple; tropical minus subtropical temperature difference) are plotted in Fig. 2.

The evolution of $\phi_{\Psi 500}$ to the abrupt forcing, does not coincide with the response of T_s (Fig. 2a). As discussed in Grise and Polvani (2017), while the response time of the Hadley cell width is ~7 years, T_s monotonically increases through the entire simulation, implying that T_s is not the main driver of the Hadley cell expansion: through most of the simulation T_s increases while the Hadley cell width does not. Nevertheless, because the atmospheric circulation is driven by vertical temperature gradients (e.g., Charney 1947; Eady 1949), the importance of T_s reported in previous studies might be related to changes in the vertical temperature profile, and not changes in T_s alone, as further discussed in section 4.

Changes in $\Delta_h T_s$ also do not coincide with the response of the Hadley cell width to the abrupt forcing

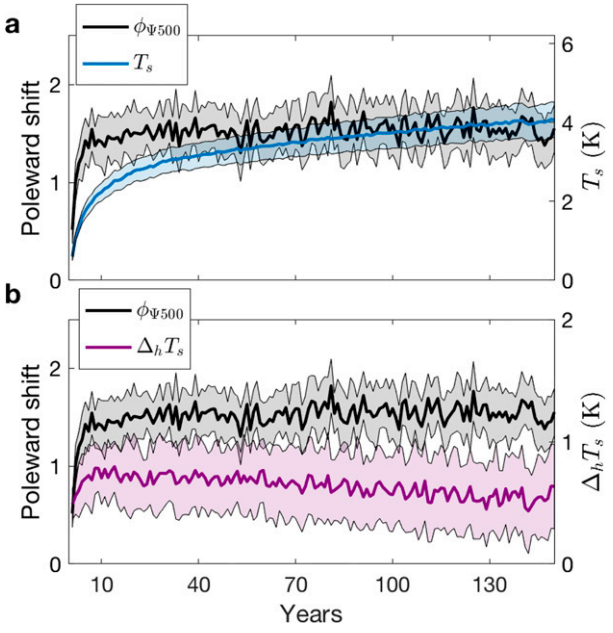

FIG. 2. The annual and zonal multimodel-mean evolution relative to preindustrial values of the Hadley cell edge $\phi_{\Psi500}$ (° lat; black lines in all panels). (a) Southern Hemisphere mean surface temperature T_s (K; blue) and (b) meridional surface temperature gradient $\Delta_h T_s$ (K; purple; difference between tropical and subtropical temperatures). The shading in both panels represents the 95% confidence interval calculated via the Student's t test across all models.

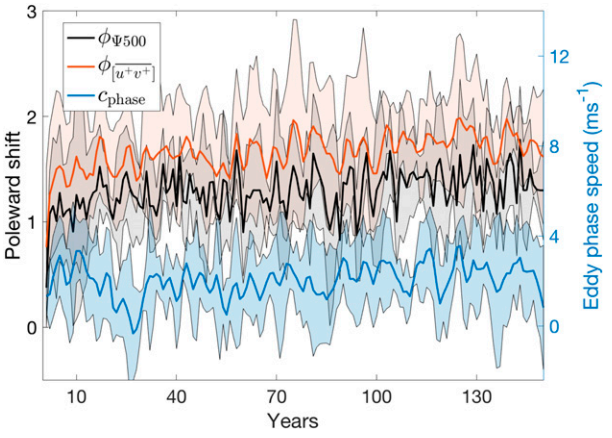

FIG. 3. (a) The annual and zonal multimodel-mean (over all models with available daily data) evolution, relative to preindustrial values, of the Hadley cell edge $\phi_{\Psi500}$ (° lat; black), the latitude of maximum eddy momentum flux $\phi_{\overline{[u^+v^+]}}$ (° lat; red), and the eddy phase speed of maximum eddy momentum flux c_{phase} (m s^{-1}; blue). The shadings represent the 95% confidence interval calculated via the Student's t test across all models. Each model data point has been smoothed with a 5-yr running mean for plotting purposes.

(Fig. 2b). In contrast to the monotonic widening of the Hadley cell, $\Delta_h T_s$ shows a nonmonotonic behavior, reaching a maximum value after ~10 years and then actually decreasing through the rest of the simulation. Thus, while there is a direct relation between $\Delta_h T_s$ and $\phi_{\Psi500}$ during the fast response (up to ~10 years), in the slow response they show an inverse relation. This might explain the direct relation between $\Delta_h T_s$ and $\phi_{\Psi500}$ found in an atmosphere-only model (Frierson et al. 2007), where slow-response processes, associated with the ocean circulation, are absent, in contrast to the inverse relation found in reanalysis data (Adam et al. 2014).

b. Eddy phase speed

Several studies (e.g., Lu et al. 2008; Ceppi and Hartmann 2013) have suggested that the increased eddy phase speed found under global warming (Chen and Held 2007) results in the poleward shift of the Hadley cell edge. Larger eddy phase speeds push the critical latitude poleward, so that eddies dissipate at higher latitudes. The associated shift of the latitude of zero eddy momentum flux divergence (i.e., the latitude where the mean meridional flow is zero) results in the widening of the Hadley cell. Again, since the above mechanism was examined by correlating the long-term response fields, the cause and effect relation remains unclear.

To determine if indeed the eddy phase speed causes the changes in latitude of maximum eddy momentum flux (which corresponds to the latitude of zero eddy momentum flux divergence) and the poleward shift of the Hadley cell edge, the evolution of $\phi_{\Psi500}$ (black), $\phi_{\overline{[u^+v^+]}}$ (red), and c_{phase} (blue) are plotted in Fig. 3. One can see that $\phi_{\overline{[u^+v^+]}}$ shifts poleward together with $\phi_{\Psi500}$, and they are highly correlated ($r = 0.68$) through the entire run (Fig. 4a) [as shown by Ceppi and Hartmann (2013) in reanalyses]. As in Chen and Held (2007), we find that with increased levels of CO_2 c_{phase} is larger compared to preindustrial values: however, note that c_{phase} shows an instantaneous increase, while $\phi_{\Psi500}$ and $\phi_{\overline{[u^+v^+]}}$ show a gradual increase in the first years followed by a more moderate change through the rest of the simulation. As a result, changes in c_{phase} have a low correlation with the poleward shift of $\phi_{\Psi500}$ and $\phi_{\overline{[u^+v^+]}}$ (Fig. 4b; $r = 0.09$). This low correlation may stem from the increase in mean zonal wind, which acts to push the critical latitude equatorward (e.g., Lu et al. 2014). This result confirms the one reported in previous studies (Wu et al. 2013; Staten et al. 2014), which also found low correlation in the time evolution of the eddy phase speed and the mean meridional circulation. Thus, the high correlation between the poleward shift of $\phi_{\Psi500}$ and $\phi_{\overline{[u^+v^+]}}$ (Fig. 4a) is not due to changes in the eddies' dissipation region inside the tropics (critical latitude, as shown in Figs. 3 and 4), but rather is due to changes in

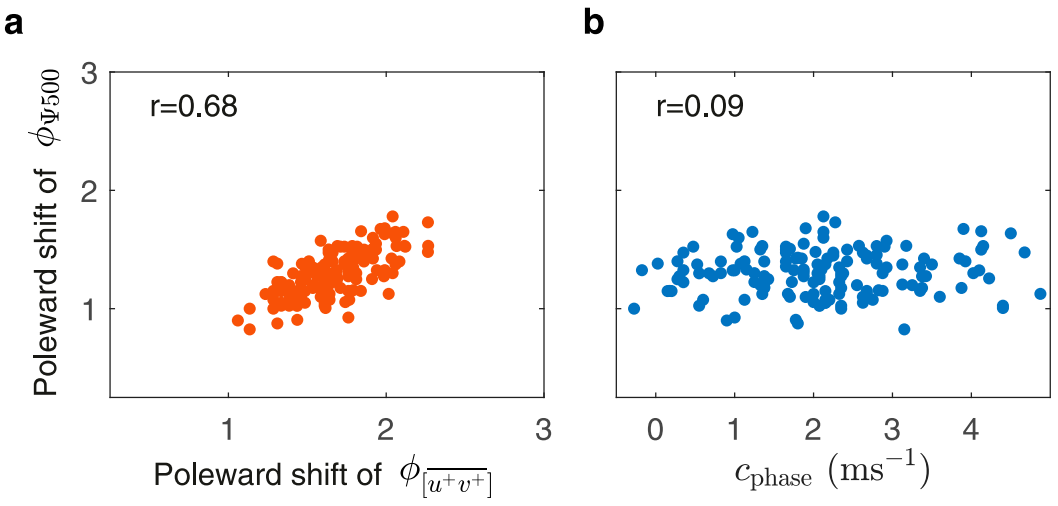

FIG. 4. The annual and zonal multimodel-mean (over all models with available daily data) response, relative to preindustrial values, of the Hadley cell edge $\phi_{\Psi 500}$ (° lat) as a function of (a) the latitude of maximum eddy momentum flux $\phi_{\overline{[u^+v^+]}}$ (° lat) and (b) the eddy phase speed of maximum eddy momentum flux c_{phase} (m s^{-1}). Each dot represents 1 year averaged over all models with available daily data.

the eddies' source region (extratropical baroclinicity), as further discussed in the next section.

4. The relative importance of the Hadley cell width scalings and their components

Having shown that T_s and c_{phase} occur on different time scales than the Hadley cell expansion, we next turn to the theories, and analyze the Held and Hou (1980) and Held (2000) scalings for the Hadley cell width. Studying the evolution of these scaling, along with their different components, will provide further insights into the physical mechanism behind the Hadley cell expansion at steady state (note that the balance at the upper branch of the Hadley cell between the annual mean meridional advection of zonal momentum and Coriolis acceleration holds through the entire simulation).

a. Comparing Hadley cell width scalings

Previous studies found that while changes in ϕ_{H00} [Eq. (2)] along with its components (subtropical static stability and tropopause height) are highly correlated with changes in $\phi_{\Psi 500}$ (Frierson et al. 2007; Lu et al. 2007, 2008; Son et al. 2018), changes in the tropical tropopause height in ϕ_{HH} [Eq. (1)] have a low correlation with changes in $\phi_{\Psi 500}$ (Lu et al. 2007). To properly examine whether indeed ϕ_{H00} better predicts $\phi_{\Psi 500}$ than ϕ_{HH}, it is crucial to first compare the entire scaling [Eqs. (1) and (2)], when all components are taken into account. As shown in Fig. 5, across all models, the zonal mean statistically steady-state poleward shifts of ϕ_{H00} indeed shows a better correlation with $\phi_{\Psi 500}$ ($r = 0.88$) than ϕ_{HH} ($r = 0.24$). Because ϕ_{H00} accounts for the role of eddies in affecting the mean circulation in the subtropics, its high correlation with $\phi_{\Psi 500}$ is not surprising, given the high correlation between $\phi_{\Psi 500}$ and $\phi_{\overline{[u^+v^+]}}$ shown above in Figs. 3 and 4a.

As the poleward shift of $\phi_{\Psi 500}$ better correlates with the poleward shift of ϕ_{H00}, the transient evolution of the latter is further examined in order to obtain a deeper understanding of the mechanisms behind the transient and steady-state widening of the Hadley cell. As one can see in Fig. 6a, ϕ_{H00} shows a similar evolution under the abrupt forcing as $\phi_{\Psi 500}$ (cf. red and black lines). It shows a rapid response in the first years that accounts for most of the expansion, followed by a more moderate poleward shift. In spite of the similar overall behavior, the evolution of ϕ_{H00} also deviates from the behavior of $\phi_{\Psi 500}$ (note that the overlapping of the confidence interval of $\phi_{\Psi 500}$ and ϕ_{H00} starts only after ~7 years, when $\phi_{\Psi 500}$ has already reached 95% of its steady-state value). In Fig. 6b, we zoom in on the first 40 years of evolution: whereas the response time of $\phi_{\Psi 500}$ is ~7 years (black line), the response time of ϕ_{H00} is ~20 years (red line). This slower increase of ϕ_{H00} relative to $\phi_{\Psi 500}$ indicates that different physical mechanisms control them, which we proceed to elucidate next.

b. The roles of static stability and tropopause height

Previous studies found that both components of the Held (2000) scaling [the tropopause height and static stability; Eq. (2)] correlate with $\phi_{\Psi 500}$ (Lu et al. 2007, 2008); this makes it difficult to quantify their relative

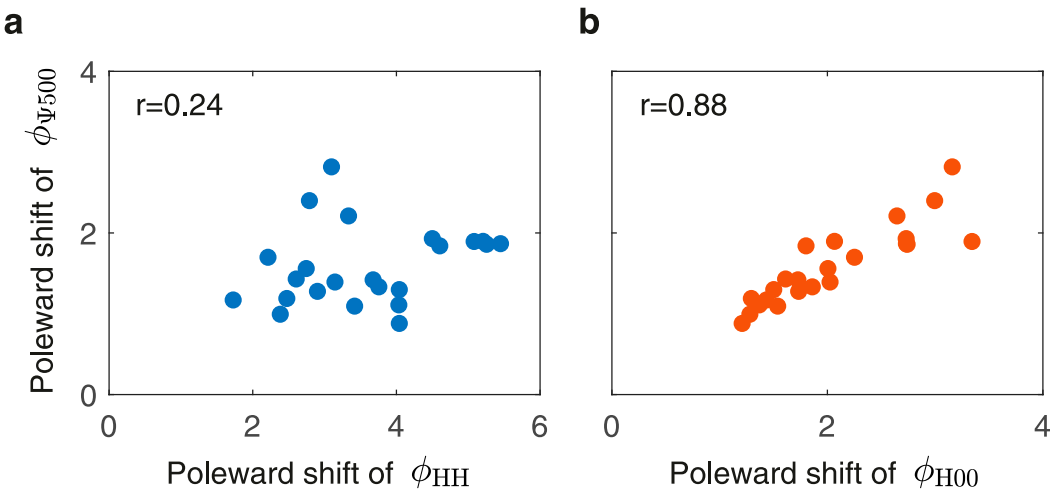

FIG. 5. The statistically steady-state Hadley cell edge $\phi_{\Psi500}$ (° lat) poleward shift, relative to preindustrial values, as a function of the poleward shift of the Hadley cell edge (° lat), based on (a) the Held and Hou (1980) scaling ϕ_{HH} [Eq. (1)], and (b) the Held (2000) scaling ϕ_{H00} [Eq. (2)]. Each dot in (a) and (b) represents one model simulation averaged over the last 50 years of simulation.

importance in shifting $\phi_{\Psi500}$ poleward. However, studying their evolution allows us to disentangle their relative roles, and sheds new light on the mechanism behind the transient and steady-state tropical expansion. In particular, we wish to understand which of these components is responsible for the rapid poleward shift that results in the similar evolution as $\phi_{\Psi500}$, and which for the slower increase that causes ϕ_{H00} to deviates from $\phi_{\Psi500}$.

Dividing Eq. (2) by its preindustrial value and taking the logarithm enables us to disentangle the components in the Held (2000) scaling, the subtropical tropopause height H_e and static stability N:

$$\log\left(\frac{\phi_{H00}}{\phi_{H00_{PI}}}\right) = 0.5\log\left(\frac{N}{N_{PI}}\right) + 0.5\log\left(\frac{H_e}{H_{e_{PI}}}\right). \quad (3)$$

The evolution of the different terms in Eq. (3) is plotted in Fig. 7a. By construction, the sum of the tropopause height term (blue line) and static stability term (green line) equals the response of ϕ_{H00} (red line). In the first ~5 years, changes in static stability and tropopause height contribute equally to the rapid poleward shift of ϕ_{H00}. While the response time of the static stability is ~10 years (similar to poleward shift of the Hadley cell), the response time of tropopause height is ~25 years (similar to poleward shift of ϕ_{H00}). Thus, after the fast response of the first years, the slower monotonic increase of the tropopause height alone contributes to the increase of ϕ_{H00}. This increase results in the deviation between the evolution of $\phi_{\Psi500}$ and ϕ_{H00} (cf. black and red lines in Fig. 6a).

What changes in the temperature field are responsible for the rapid and slow responses of ϕ_{H00}? Both an increase in tropospheric temperature, relative to the lower stratosphere, and a decrease in temperature lapse rate increase the tropopause height [e.g., Thuburn and Craig 2000; see also Eq. (9) in Vallis et al. (2015)]. In addition, a decrease in temperature lapse rate stabilizes the atmosphere, thus increasing the static stability. Plotting the evolution of subtropical temperature at various levels shows that the upper troposphere (400–600 hPa; blue line in Fig. 7b) warms faster than the lower troposphere (600–850 hPa; red line in Fig. 7b) in the first ~15 years, after which they both warm at approximately the same rate. As a consequence, the response time of the tropospheric vertical temperature difference (green line in Fig. 7b), calculated between the upper and lower troposphere, is ~14 years. This explains the rapid response of both the static stability (green line in Fig. 7a) and tropopause height (blue line in Fig. 7a). The continued monotonic increase in tropospheric temperature (relative to the slower increase in lower-stratospheric temperature, black line) further increases the tropopause height (blue line in Fig. 7a), leading ϕ_{H00} to a response time of ~20 years, and thus to deviate from $\phi_{\Psi500}$.

To more clearly illustrate the effect of the tropopause height on ϕ_{H00}, the latter is recalculated using constant preindustrial tropopause height values $\phi_{H00|_{H_{PI}}}$ (green line in Fig. 6), so that only changes in static stability affect the widening of the Hadley cell. One can see that $\phi_{H00|_{H_{PI}}}$ better follows the poleward shift of $\phi_{\Psi500}$ (cf. black and green lines in Fig. 6). Unlike ϕ_{H00}, which has a

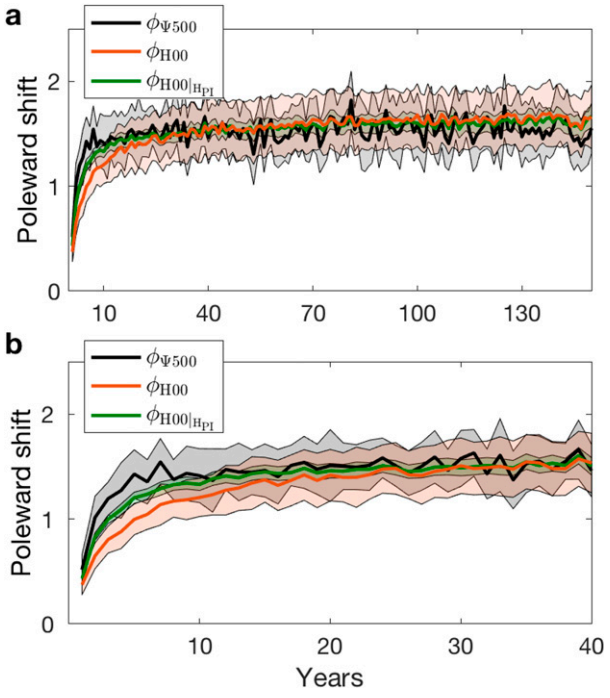

FIG. 6. (a) The annual and zonal multimodel-mean evolution relative to preindustrial values of the Hadley cell edge $\phi_{\Psi 500}$ (° lat; black line), the Hadley cell edge based on Held (2000) scaling ϕ_{H00} [° lat; red line; Eq. (2), using constant of proportionality of 0.8], and the Hadley cell edge based on Held (2000) scaling but with keeping tropopause height as in preindustrial values $\phi_{\mathrm{H00}|_{H_{\mathrm{PI}}}}$ (° lat; green line, using constant of proportionality of 2). (b) As in (a), but only focusing on the first 40 years. The shading in both panels represents the 95% confidence interval calculated via the Student's t test across all models.

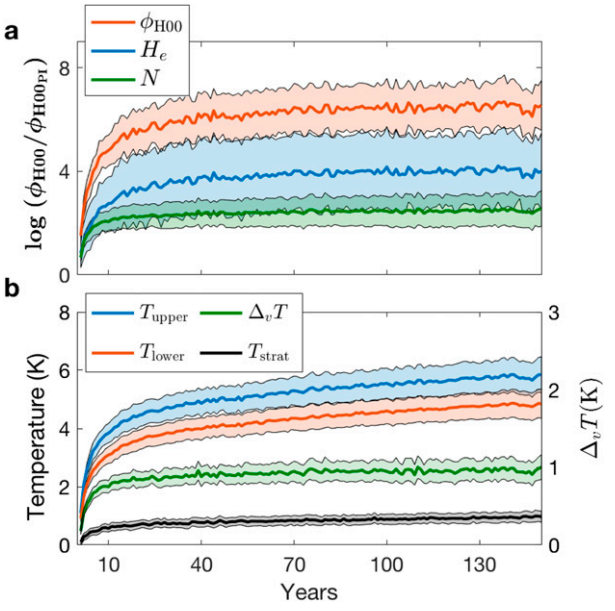

FIG. 7. (a) The evolution of the log of the ratio of the annual and zonal multimodel-mean Hadley cell edge based on Held (2000) scaling ϕ_{H00} [red; Eq. (3)], subtropical tropopause height (blue), and static stability (green) with their corresponding preindustrial values. (b) Changes relative to preindustrial values in annual and zonal multimodel-mean subtropical upper-troposphere temperature (K; blue; 400–600 hPa), lower-troposphere temperature (K, red, 600–850 hPa), lower-stratosphere temperature (K; black; 100–200 hPa), and the vertical tropospheric temperature difference (K; green) as a function of time. The shading in all panels represents the 95% confidence interval calculated via the Student's t test across all models.

response time of ~20 years, $\phi_{\mathrm{H00}|_{H_{\mathrm{PI}}}}$ has a response time of ~10 years, similar to the response time of $\phi_{\Psi 500}$. This shows the importance of the static stability, and not the tropopause height, in shifting the Hadley cell poleward.

c. *Changes in subtropical baroclinicity*

How come the tropopause height causes the response of ϕ_{H00} to deviate from the response of $\phi_{\Psi 500}$? In the Held (2000) theory, an increase in tropopause height should increase the critical shear necessary for baroclinic instability, according to the two-layer model (Phillips 1954), and thus push poleward the latitude where it is equal to the angular momentum conserving shear. One possibility is that the subtropical baroclinicity in the atmosphere is insensitive to the tropopause height.

To examine this possibility, a linear normal-mode instability analysis is conducted following Smith (2007), which was found to capture the baroclinic properties of eddies in both GCMs and reanalysis data (Jansen and Ferrari 2012; Chemke and Kaspi 2015, 2016a,b; Chemke et al. 2016). In this analysis the eigenvalue problem of the linearized quasigeostrophic potential vorticity (QGPV) equation is numerically solved at each latitude, using each model's mean zonal wind, static stability, and tropopause height. The tropopause height sets the upper boundary of the problem. The resulting growth rates of the eddies are used as a measure for baroclinicity. First, the subtropical growth rate (the mean of the growth rate over all wavenumbers averaged over the subtropics) is calculated for each model using the zonal- and annual-mean fields of the preindustrial and of the statistically steady-state abrupt $4 \times CO_2$ runs (last 50 years). Then, the growth rate of the statistically steady-state abrupt $4 \times CO_2$ run is recalculated, but with the tropopause height in preindustrial values.

The difference in the growth rate between the $4 \times CO_2$ and preindustrial runs is plotted against the difference between the $4 \times CO_2$ run using the preindustrial tropopause height and preindustrial run (Fig. 8a). First, most of the models (17) show a decrease in the growth rate relative to preindustrial values (y axis in Fig. 8), with a multimodel mean value of $-1.1 \times 10^{-7}\,\mathrm{s}^{-1}$ (red

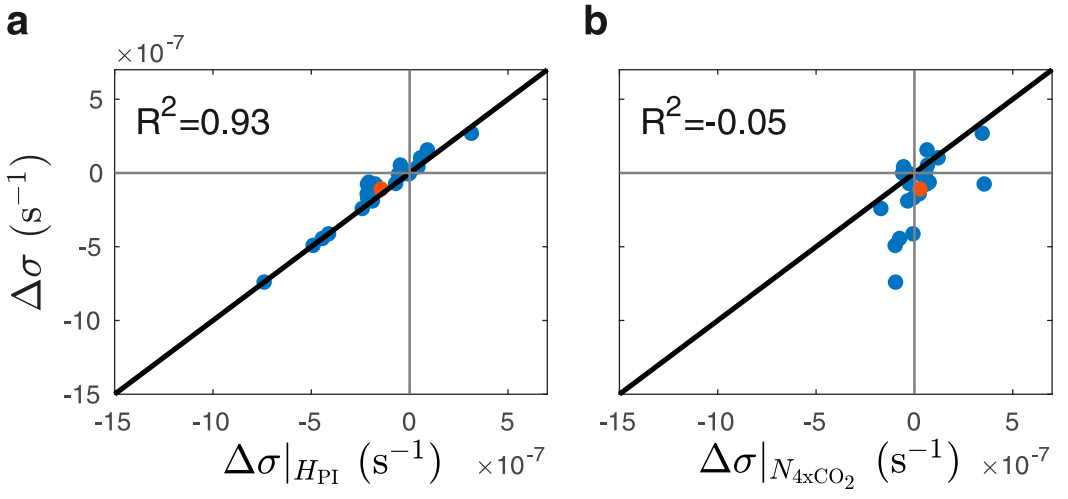

FIG. 8. Changes relative to preindustrial values in mean (averaged over all wavenumbers) subtropical growth rate $\Delta\sigma$ (s^{-1}) as a function of (a) changes in growth rate while holding tropopause height in preindustrial values $\Delta\sigma|H_{PI}$ and (b) changes in growth rate while holding static stability in 4 × CO_2 values $\Delta\sigma|_{N_{4\times CO_2}}$. Each dot in (a) and (b) represents one model simulation averaged over the last 50 years of the 4 × CO_2 run and over the last 200 years of the preindustrial run. Growth rates are calculated at the subtropics, by solving the linearized quasigeostrophic potential vorticity equation following Smith (2007). In both panels, the coefficient of determination is calculated relative to the 1:1 ratio lines (black lines). The red dots show the multimodel-mean value.

dot). This indicates that the baroclinicity decreases under the abrupt 4 × CO_2 forcing. Second, if the tropopause height affects the growth rate, the dots in Fig. 8a should not fall on the 1:1 line (black line). However, in most models changes in growth rate are similar (blue dots on the 1:1 line; $R^2 = 0.93$) whether or not the tropopause height is allowed to increase from preindustrial values. Thus, changes in tropopause height in the 4 × CO_2 simulations have a minor effect on baroclinicity.

In contrast, static stability changes have a large effect: the difference in the growth rate between the 4 × CO_2 and preindustrial runs is plotted against the difference between the 4 × CO_2 and preindustrial runs using the 4 × CO_2 static stability values (Fig. 8b). Using fixed 4 × CO_2 static stability values rather than preindustrial values, as was done for the tropopause height, precludes including stratospheric static stability values for the 4 × CO_2 calculation, when the tropopause height increases. Keeping the static stability at abrupt 4 × CO_2 values yields changes in baroclinicity that are different than when allowing the static stability to change (dots do not fall on the 1:1 line in Fig. 8b; $R^2 = -0.05$). In addition, keeping the static stability constant results in minor changes in baroclinicity in most models (dots fall close to the *x*-axis zero line, with multimodel mean value of $2.8 \times 10^{-8}\,m^{-1}\,s^{-1}$; red dot). Thus, the increase in subtropical static stability explains most of the decrease in subtropical baroclinicity as the climate becomes warmer.

In summary, the rapid increase of static stability (i.e., rapid decrease of the subtropical lapse rate) in the first ~10 years decreases the baroclinicity, and explains most of the poleward shift of the Hadley cell and of the eddy momentum flux. The tropopause height, on the other hand, seems to have a minor effect on baroclinicity, and thus shows different response time than the Hadley cell width. This result is in agreement with the results of Son et al. (2018), who found high correlation between changes in subtropical static stability and Hadley cell shift in past and projected climates.

d. Applicability to more realistic scenarios

The above analyses are conducted using the abrupt 4 × CO_2 forcing. The abrupt change in CO_2 helps disentangle the different response times of the different components that affect the Hadley cell expansion, and thus provides better understanding of the controlling mechanisms. In a more realistic scenario, however, CO_2 increases continuously. To examine the above results in such a realistic scenario, the 1% CO_2 increase per year scenario is now investigated. Figure 9a is similar to Fig. 6a, only showing the evolution under the 1% CO_2 increase per year scenario, relative to preindustrial values, of the poleward shift of $\phi_{\Psi 500}$ (black), ϕ_{H00} [red; Eq. (2)], and $\phi_{H00|_{H_{PI}}}$ (green). Unlike for the abrupt CO_2 forcing, $\phi_{\Psi 500}$ does not reach a statistically steady state value, but rather monotonically shifts poleward, due to the gradual increase in CO_2. Toward the end of the simulation, ϕ_{H00} shifts more poleward than $\phi_{\Psi 500}$ and

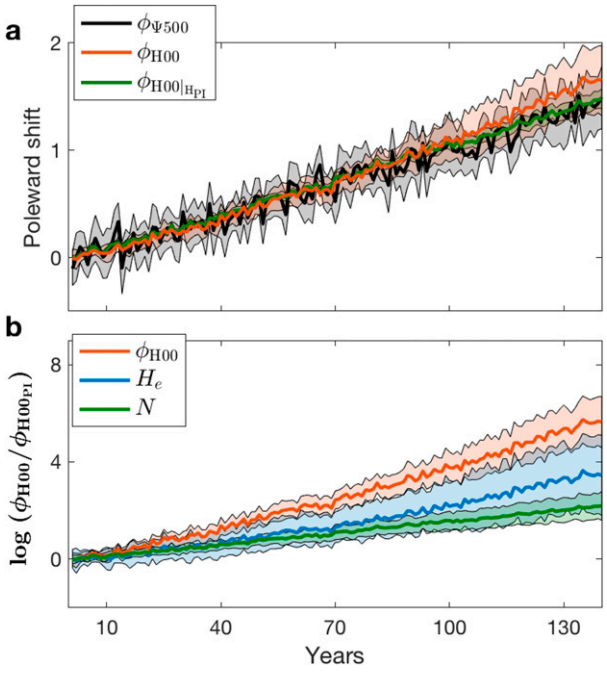

FIG. 9. (a) The annual and zonal multimodel-mean evolution, from the 1% yr^{-1} increase in CO_2, relative to preindustrial values of the Hadley cell edge $\phi_{\Psi 500}$ (° lat; black), the Hadley cell edge based on Held (2000) scaling ϕ_{H00} [° lat; red; Eq. (2)] and the Hadley cell edge based on Held (2000) scaling but with keeping tropopause height as in preindustrial values (green; ° lat). (b) Evolution of the log of the ratio of the annual and zonal multimodel mean, from the 1% yr^{-1} increase in CO_2, Hadley cell edge based on Held (2000) scaling [black; Eq. (3)], subtropical tropopause height (blue), and static stability (red) with their corresponding preindustrial values as a function of time. The shading in all panels represents the 95% confidence interval calculated via the Student's *t* test across all models.

$\phi_{\mathrm{H00}|_{H_{\mathrm{PI}}}}$. Note that in spite of the overlapping confidence intervals of $\phi_{\Psi 500}$ and ϕ_{H00} there is a clear separation of the multimodel ensemble means that increases with time. Similar to the abrupt 4 × CO_2 experiment, this shows that the disagreement of ϕ_{H00} and $\phi_{\Psi 500}$ stems from tropopause height changes.

To see the different responses of static stability and tropopause height in the 1% CO_2 increase per year scenario, the different terms of Eq. (3) are plotted in Fig. 9b. By construction, the sum of the change in static stability (green) and tropopause height (blue) equals the change in ϕ_{H00} (red). Similar to the abrupt 4 × CO_2 experiment, at the beginning of the run (up to year ~70) both static stability and tropopause height contribute equally to the poleward expansion of ϕ_{H00}. Then, the tropopause height increases faster than the static stability (as it is also affected by the warming of the troposphere relative to the lower stratosphere), which further pushes poleward ϕ_{H00}, causing it to deviate from the poleward shift of $\phi_{\Psi 500}$. This again shows the importance of the static stability, and not the tropopause height, in shifting the Hadley cell edge poleward.

5. Edge of the dry zone

Another important metric for the edge of the tropics is the latitude where precipitation equals evaporation ϕ_{P-E} (edge of the dry zone). Unlike the Hadley cell edge, this metric holds information regarding the hydrological cycle, as it separates regions of net evaporation (the dry zone) from regions of net precipitation (midlatitudes). Thus, this metric is important in assessing the effects of climate change on the hydrological cycle. Recently, Grise and Polvani (2017) and Seviour et al. (2018) showed that the evolution of $\phi_{\Psi 500}$ deviates from the poleward shift of ϕ_{P-E}. While several studies found the response of these two metrics to be highly correlated across a large set of models (e.g., Lu et al. 2007; Polvani et al. 2011b; Quan et al. 2014; Solomon et al. 2016), their different time evolutions suggest that different physical mechanisms control them.

The evolution of $\phi_{\Psi 500}$ (black line) and ϕ_{P-E} (blue line) to the abrupt 4 × CO_2 forcing are plotted in Fig. 10a. In the first years ϕ_{P-E} shows a rapid poleward shift as $\phi_{\Psi 500}$, after which it shows a slower poleward shift. As discussed in Grise and Polvani (2017), whereas the response time of $\phi_{\Psi 500}$ is ~7 years, the response time of ϕ_{P-E} is ~20 years. By studying the zonal- and annual-mean vertically integrated moisture budget, Grise and Polvani (2017) showed that the poleward shift of the Hadley cell edge (mean meridional velocity) and changes in transient eddy moisture flux divergence, contribute, respectively, to the fast and slow responses of the dry zone edge. Here, we further elaborate on the results of Grise and Polvani (2017) and analyze the subtropical moisture budget by including the effects of stationary eddies and zonal mean flow.

Following Trenberth and Guillemot (1995) and Seager et al. (2010), changes of the zonal- and annual-mean vertically integrated subtropical moisture budget, can be written as follows:

$$\delta[\overline{E}-\overline{P}] = \frac{1}{ga\cos\phi}\frac{\partial}{\partial\phi}\left(\int_o^{p_s}\delta[\overline{v}][\overline{q}]\cos\phi + \delta\overline{[v^+q^+]}\cos\phi\, dp\right), \tag{4}$$

where δ represents the transient response, E and P are the evaporation from the surface and precipitation, respectively, and q is specific humidity. While the first term on the right-hand side accounts for changes in mean moisture flux, the second term accounts for changes in eddy moisture flux (deviation from both zonal and monthly means).

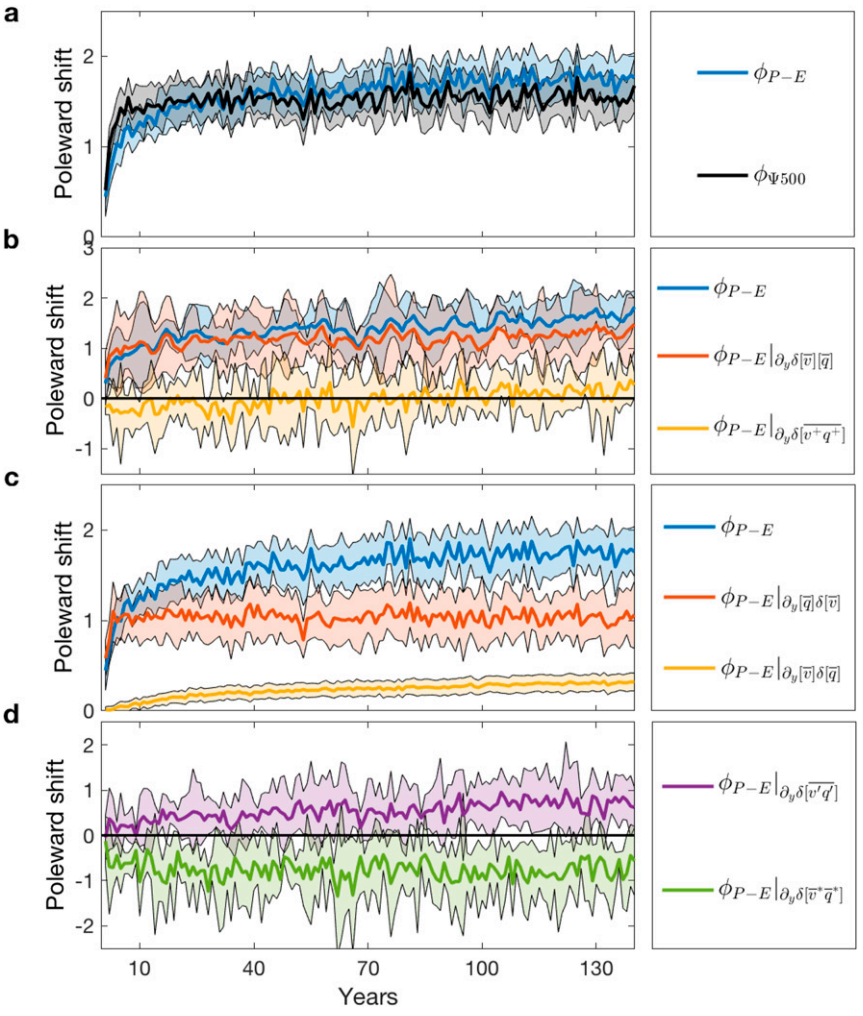

FIG. 10. The annual and zonal multimodel-mean evolution relative to preindustrial values of (a) the latitude where precipitation equals evaporation ϕ_{P-E}; (° lat; blue) and the Hadley cell edge $\phi_{\Psi 500}$ (° lat; black); (b) the contribution of the divergence of mean meridional moisture flux (red) and the divergence of total (transient and stationary) eddy moisture flux (yellow) to the shift of ϕ_{P-E} (blue); (c) the contribution of the divergence of mean meridional moisture flux to the shift of ϕ_{P-E} (blue) decomposed to changes arising from circulation (red) and moisture (yellow); and (d) the contribution of the divergence of total eddy moisture flux to the shift of ϕ_{P-E} decomposed to changes arising from transient eddies (purple) and stationary eddies (green). The shading in all panels represents the 95% confidence interval calculated via the Student's *t* test across all models. In (b) and (d) all models with available daily data have been used, and each model data point has been smoothed with a 3-yr running mean for plotting purposes.

Plotting the evolution of the contribution of the right-hand side terms in Eq. (4) to the shift of ϕ_{P-E} shows that most of the response of ϕ_{P-E} (blue line in Fig. 10b) is associated with changes $[\overline{v}][\overline{q}]$ alone (red line in Fig. 10b). The meridional divergence of $\overline{[v^+q^+]}$ (yellow line in Fig. 10b), on the other hand, shows minor changes to quadrupling CO_2, and thus does not contribute to the increase in ϕ_{P-E}. The response of $[\overline{v}][\overline{q}]$ can be further decomposed as follows:

$$\delta[\overline{v}][\overline{q}] \approx [\overline{q}]\delta[\overline{v}] + [\overline{v}]\delta[\overline{q}], \tag{5}$$

where the first term on the right-hand side accounts for changes in circulation and the second term accounts for changes in moisture itself (Held and Soden 2006; Seager et al. 2010).

Plotting the evolution of the contribution of the meridional divergence of the right-hand side of Eq. (5) to the shift of ϕ_{P-E} shows that changes in circulation (red

line in Fig. 10c) and in moisture (yellow line in Fig. 10c) have different time evolutions, and thus play different roles in shifting ϕ_{P-E}. While changes in circulation have a rapid response, with a response time of ~4 years (as discussed in section 3), changes in moisture are slower and constantly increasing, with a response time of ~100 years. This suggests that the initial fast poleward shift of ϕ_{P-E} is driven by the rapid expansion of the Hadley cell (which is driven by the fast response of the subtropical lapse rate, as discussed in section 4b), and that its slower monotonic shift is driven by changes in moisture content. At the end of the simulation, ~75% of the poleward shift of the dry zone edge is due to the widening of the Hadley cell, and ~25% due to the increase in subtropical moisture. This is similar to the results of Scheff and Frierson (2012), who found that most of the drying in subtropical regions stems from the poleward shift of the mean meridional circulation, and not from changes in moisture content.

To better understand the minor contribution of eddy moisture flux to the poleward shift of the dry zone edge (yellow line in Fig. 10b), the response of the eddy moisture flux is further decomposed as follows:

$$\delta[\overline{v^+q^+}] = \delta[\overline{v'q'}] + \delta[\overline{v}^*\overline{q}^*], \tag{6}$$

where the first and second terms represent changes in transient (purple line in Fig. 10d) and stationary (green line in Fig. 10d) eddies, respectively. As discussed in Grise and Polvani (2017) and Seager et al. (2010), the divergence of transient eddy moisture flux (purple) acts to push ϕ_{P-E} poleward. Here we show that the divergence of stationary eddy moisture flux (green), on the other hand, acts to push ϕ_{P-E} equatorward. The cancelation of the transient and stationary eddy moisture fluxes (as was found under regional warming in the Northern Hemisphere; Shaw and Voigt 2016) results in a minor contribution of the eddy fields to the poleward shift of ϕ_{P-E}.

What causes the different behavior of transient and stationary eddy moisture fluxes? Figure 11 shows the vertically integrated, multimodel, zonal-mean latitudinal structure of the transient (Figs. 11a,c) and stationary (Figs. 11b,d) eddy moisture flux in the preindustrial run (red lines) and the statistically steady-state 4 × CO_2 run (blue lines). Both transient and stationary eddy moisture flux are negative, as they act to transfer moisture from the tropics toward the South Pole (Figs. 11a,b). While the transient eddy moisture flux reaches maximum value at midlatitudes (~40°S), the stationary eddy moisture flux reaches maximum value in the lower subtropics (~25°S), where most of the Southern Hemisphere continents reside. Because of their different latitudinal structures, the transient eddy moisture flux tend to diverge moisture in the subtropics (positive values in Fig. 11c), while the stationary eddy moisture flux tends to converge moisture in the subtropics (negative values in Fig. 11d). Under increased CO_2 concentrations, both the transient and stationary eddy moisture fluxes shift poleward (cf. red and blue lines in Figs. 11a and 11b). Thus, a poleward shift of the transient eddy moisture flux increases its divergence in the subtropics, while a poleward shift of the stationary eddy moisture flux increases its convergence in the subtropics (cf. red and blue lines in Figs. 11c and 11d), resulting in opposite tendencies, as shown in Fig. 10d, that lead to the total cancelation in the subtropics.

6. Summary

The projected widening of the tropical circulation with increased greenhouse gases (e.g., Lu et al. 2007; Vallis et al. 2015) and the associated shift of the dry zone edge have important societal impacts. Several mechanisms have been suggested to explain this poleward shift, but the coupling among the different atmospheric components did not allow for a quantification of their relative importance in expanding the tropics. Here, using the abrupt quadruple-CO_2 scenario runs from the CMIP5, we have been able to separate the relevant mechanisms of tropical expansion. The different response times of the various mechanisms has enabled us to disentangle the different components in question and elucidate their relative importance.

Upon abrupt 4 × CO_2, the Hadley cell rapidly expands poleward, with a response time of ~7 years (Grise and Polvani 2017). Confirming several earlier studies (e.g., Frierson et al. 2007; Lu et al. 2007, 2008), we find that this expansion can be explained with the Held (2000) theory, where changes in subtropical baroclinicity control the width of the Hadley cell. In addition, we have shown that a rapid increase in static stability (i.e., decrease in the subtropical lapse rate) in the first few years of the simulation leads to the rapid poleward shift of the Hadley cell edge. This was found to occur in both the abrupt 4 × CO_2 and the 1% yr^{-1} increase forcing. Changes in tropopause height, however, were found to divert the poleward shift of the Held (2000) theory from that of the Hadley cell edge. Unlike the static stability, the increase in tropopause height was found to have a minor effect on subtropical baroclinicity, and thus on the widening of the tropical belt.

Changes in subtropical baroclinicity also affect subtropical eddy fields. As in Ceppi and Hartmann (2013), we find that the poleward shift of the Hadley cell is indeed highly correlated with the poleward shift of subtropical eddy momentum flux. Several studies have suggested that this correlation might not be solely due to

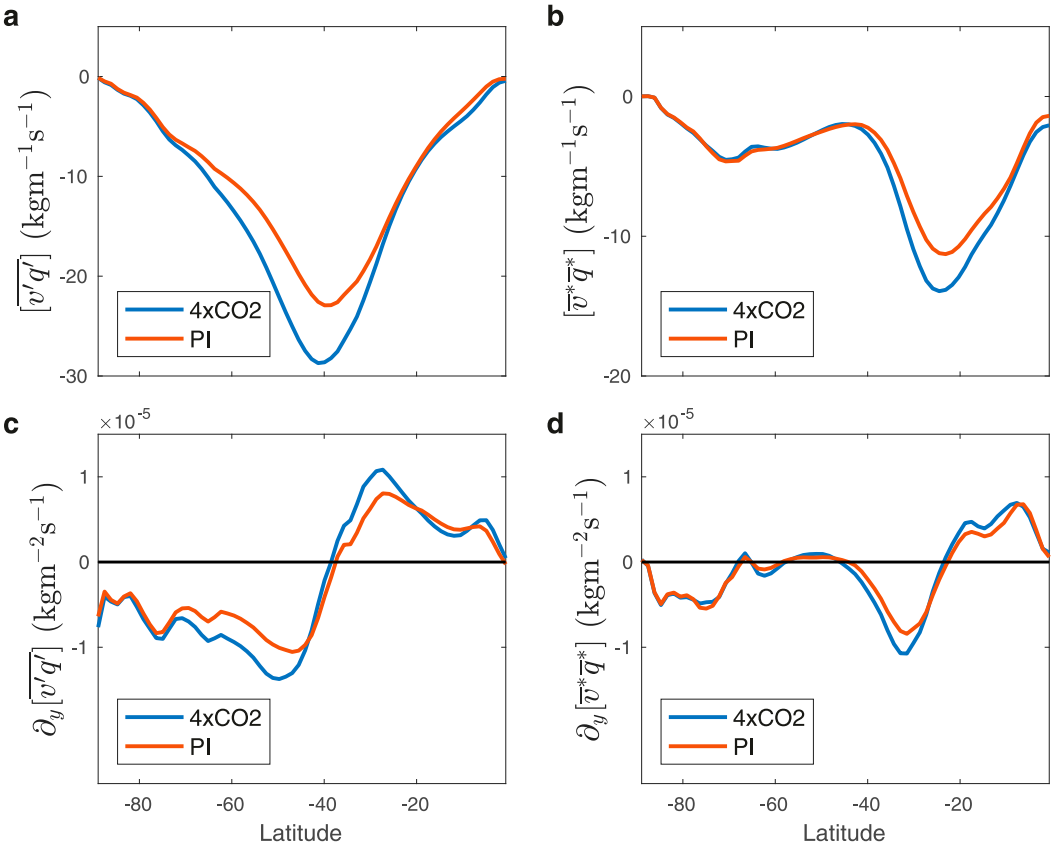

FIG. 11. The annual and zonal vertically integrated multimodel-mean (over all models with available daily data) (a) transient eddy moisture flux ($\mathrm{kg\,m^{-1}\,s^{-1}}$), (b) stationary eddy moisture flux ($\mathrm{kg\,m^{-1}\,s^{-1}}$), (c) meridional divergence of transient eddy moisture flux ($\mathrm{kg\,m^{-2}\,s^{-1}}$), and (d) meridional divergence of stationary eddy moisture flux ($\mathrm{kg\,m^{-2}\,s^{-1}}$) as a function of latitude. In all panels, the red and blue lines respectively represent the preindustrial run and the average over last 50 years of the abrupt $4 \times CO_2$ forcing run.

changes in eddy generation (i.e., baroclinicity) outside the tropics, but also due to an increase in eddy phase speed, which pushes the critical latitude poleward (where eddies dissipate) together with the subtropical eddy momentum flux. Here, however, we have shown that the increase of the eddy phase speed under abrupt $4 \times CO_2$ (e.g., Chen and Held 2007) does not correlate with the poleward shift of the Hadley cell edge. And, more importantly, changes in global-mean surface temperature and meridional surface temperature gradient were also found not to accompany changes in Hadley cell width.

Unlike the poleward shift of the Hadley cell edge, which is relatively fast, the poleward shift of the dry zone edge has a slower time response, and monotonically increases throughout the simulation (Grise and Polvani 2017; Seviour et al. 2018). In the first few years after CO_2 quadrupling the rapid poleward movement of the Hadley cell edge shifts the dry zone edge poleward. This accounts for most of the poleward shift of the dry zone edge. The slower increase in moisture further pushes the dry zone edge poleward through the rest of the run. Eddy moisture flux was found to have a minor contribution to shifting the dry zone edge poleward, due to the cancelling effects of transient and stationary eddies, which, respectively, diverge and converge moisture in the subtropics.

The widening of the Hadley cell is only one example of circulation changes under increased CO_2 concentrations. For each of these circulation changes, one can find several mechanisms in the literature. Having several mechanisms for one physical phenomenon stems from the difficulty of isolating any causality in such a coupled and complex system, which leads to develop mechanisms based on correlating the long-term fields. However, studying the evolution of the different components in the atmosphere to an abrupt and strong forcing allows taking a step toward causality, and thus having better physical understanding of the climate system.

It is important to note that the key role of static stability that we have found in our study, that of modulating

the Hadley cell edge under increased greenhouse gases, does not necessarily apply under different forcings. For example, analyzing different idealized warming patterns, Tandon et al. (2013) argued that the wind shear, and not static stability, is most important for changing subtropical baroclinicity and the edge of the Hadley cell. Thus, the widening of the circulation in recent years, which is likely driven by both internal variability (Allen et al. 2014; Quan et al. 2014; Lucas and Nguyen 2015; Allen and Kovilakam 2017; Mantsis et al. 2017) and different forcing agents (Allen et al. 2012, 2014; Waugh et al. 2015), may stem from other components and not only from static stability. Nonetheless, the main result of our study is that subtropical static stability is key to tropical expansion under increased CO_2 concentrations. In accordance with our results, Shaw and Tan (2018) have recently demonstrated the importance of subtropical changes in modulating the width of the Hadley cell under increased greenhouse gases.

Finally, the next step for fully understanding the widening of the Hadley cell under increased greenhouse gases should focus on elucidating the different warming rates in the lower and upper subtropical troposphere (i.e., the increase in static stability). To accomplish that, as was done in Chemke and Polvani (2018), one has to analyze the thermodynamic equation and quantify for the different terms that affect the temperature field. Currently, only one of the CMIP5 models provides all the terms needed to analyze the thermodynamic equation, but this is not sufficient for disentangling the natural variability and the model biases from the forced response.

Acknowledgments. This research was supported by the NOAA Climate and Global Change Postdoctoral Fellowship Program, administered by UCAR's Cooperative Programs for the Advancement of Earth System Science (CPAESS). We acknowledge the WCRP's Working Group on Coupled Modeling, which is responsible for CMIP, and we thank the climate modeling groups (listed in Table 1) for producing and making available their model output. For CMIP the U.S. Department of Energy's PCMDI provides coordinating support and led development of software infrastructure in partnership with the Global Organization for Earth System Science Portals. LMP is grateful for the continued support of the U.S. National Science Foundation.

REFERENCES

Adam, O., T. Schneider, and N. Harnik, 2014: Role of changes in mean temperatures versus temperature gradients in the recent widening of the Hadley circulation. *J. Climate*, **27**, 7450–7461, https://doi.org/10.1175/JCLI-D-14-00140.1.

Allen, R. J., and O. Ajoku, 2016: Future aerosol reductions and widening of the northern tropical belt. *J. Geophys. Res.*, **121**, 6765–6786, https://doi.org/10.1002/2016JD024803.

——, and M. Kovilakam, 2017: The role of natural climate variability in recent tropical expansion. *J. Climate*, **30**, 6329–6350, https://doi.org/10.1175/JCLI-D-16-0735.1.

——, S. C. Sherwood, J. R. Norris, and C. S. Zender, 2012: Recent Northern Hemisphere tropical expansion primarily driven by black carbon and tropospheric ozone. *Nature*, **485**, 350–354, https://doi.org/10.1038/nature11097.

——, J. R. Norris, and M. Kovilakam, 2014: Influence of anthropogenic aerosols and the Pacific decadal oscillation on tropical belt width. *Nat. Geosci.*, **7**, 270–274, https://doi.org/10.1038/ngeo2091.

Archer, C. L., and K. Caldeira, 2008: Historical trends in the jet streams. *Geophys. Res. Lett.*, **35**, L08803, https://doi.org/10.1029/2008GL033614.

Barnes, E. A., N. W. Barnes, and L. M. Polvani, 2014: Delayed Southern Hemisphere climate change induced by stratospheric ozone recovery, as projected by the CMIP5 models. *J. Climate*, **27**, 852–867, https://doi.org/10.1175/JCLI-D-13-00246.1.

Bony, S., G. Bellon, D. Klocke, S. Sherwood, S. Fermepin, and S. Denvil, 2013: Robust direct effect of carbon dioxide on tropical circulation and regional precipitation. *Nat. Geosci.*, **6**, 447–451, https://doi.org/10.1038/ngeo1799.

Ceppi, P., and D. L. Hartmann, 2013: On the speed of the eddy-driven jet and the width of the Hadley cell in the Southern Hemisphere. *J. Climate*, **26**, 3450–3465, https://doi.org/10.1175/JCLI-D-12-00414.1.

Charney, J. G., 1947: The dynamics of long waves in a baroclinic westerly current. *J. Meteor.*, **4**, 136–162, https://doi.org/10.1175/1520-0469(1947)004<0136:TDOLWI>2.0.CO;2.

Chemke, R., and Y. Kaspi, 2015: The latitudinal dependence of atmospheric jet scales and macroturbulent energy cascades. *J. Atmos. Sci.*, **72**, 3891–3907, https://doi.org/10.1175/JAS-D-15-0007.1.

——, and ——, 2016a: The effect of eddy–eddy interactions on jet formation and macroturbulent scales. *J. Atmos. Sci.*, **73**, 2049–2059, https://doi.org/10.1175/JAS-D-15-0375.1.

——, and ——, 2016b: The latitudinal dependence of the oceanic barotropic eddy kinetic energy and macroturbulence energy transport. *Geophys. Res. Lett.*, **43**, 2723–2731, https://doi.org/10.1002/2016GL067847.

——, and L. M. Polvani, 2018: Ocean circulation reduces the Hadley cell response to increased greenhouse gases. *Geophys. Res. Lett.*, **45**, 9197–9205, https://doi.org/10.1029/2018GL079070.

——, T. Dror, and Y. Kaspi, 2016: Barotropic kinetic energy and enstrophy transfers in the atmosphere. *Geophys. Res. Lett.*, **43**, 7725–7734, https://doi.org/10.1002/2016GL070350.

Chen, G., and I. M. Held, 2007: Phase speed spectra and the recent poleward shift of Southern Hemisphere surface westerlies. *Geophys. Res. Lett.*, **34**, L21805, https://doi.org/10.1029/2007GL031200.

D'Agostino, R., and P. Lionello, 2017: Evidence of global warming impact on the evolution of the Hadley circulation in ECMWF centennial reanalyses. *Climate Dyn.*, **48**, 3047–3060, https://doi.org/10.1007/s00382-016-3250-0.

Davis, N., and T. Birner, 2017: On the discrepancies in tropical belt expansion between reanalyses and climate models and among tropical belt width metrics. *J. Climate*, **30**, 1211–1231, https://doi.org/10.1175/JCLI-D-16-0371.1.

Davis, S. M., and K. H. Rosenlof, 2012: A multidiagnostic intercomparison of tropical-width time series using reanalyses and satellite observations. *J. Climate*, **25**, 1061–1078, https://doi.org/10.1175/JCLI-D-11-00127.1.

Dunne, J. P., and Coauthors, 2012: GFDL's ESM2 global coupled climate–carbon Earth system models. Part I: Physical formulation

and baseline simulation characteristics. *J. Climate*, **25**, 6646–6665, https://doi.org/10.1175/JCLI-D-11-00560.1.

Eady, E. T., 1949: Long waves and cyclone waves. *Tellus*, **1**, 33–52, https://doi.org/10.3402/tellusa.v1i3.8507.

Frierson, D. M. W., J. Lu, and G. Chen, 2007: Width of the Hadley cell in simple and comprehensive general circulation models. *Geophys. Res. Lett.*, **34**, L18804, https://doi.org/10.1029/2007GL031115.

Fu, Q., C. M. Johanson, J. M. Wallace, and T. Reichler, 2006: Enhanced mid-latitude tropospheric warming in satellite measurements. *Science*, **312**, 1179, https://doi.org/10.1126/science.1125566.

Grise, K. M., and L. M. Polvani, 2017: Understanding the time scales of the tropospheric circulation response to abrupt CO_2 forcing in the Southern Hemisphere: seasonality and the role of the stratosphere. *J. Climate*, **30**, 8497–8515, https://doi.org/10.1175/JCLI-D-16-0849.1.

Held, I. M., 2000: The general circulation of the atmosphere. Program in Geophysical Fluid Dynamics, Woods Hole Oceanographic Institute, 179 pp., https://darchive.mblwhoilibrary.org/handle/1912/15.

——, and A. Y. Hou, 1980: Nonlinear axially symmetric circulations in a nearly inviscid atmosphere. *J. Atmos. Sci.*, **37**, 515–533, https://doi.org/10.1175/1520-0469(1980)037<0515:NASCIA>2.0.CO;2.

——, and B. J. Soden, 2006: Robust responses of the hydrological cycle to global warming. *J. Climate*, **19**, 5686–5699, https://doi.org/10.1175/JCLI3990.1.

Hu, Y., and Q. Fu, 2007: Observed poleward expansion of the Hadley circulation since 1979. *Atmos. Chem. Phys.*, **7**, 5229–5236, https://doi.org/10.5194/acp-7-5229-2007.

——, L. Tao, and J. Liu, 2013: Poleward expansion of the Hadley circulation in CMIP5 simulations. *Adv. Atmos. Sci.*, **30**, 790–795, https://doi.org/10.1007/s00376-012-2187-4.

Hudson, R. D., M. F. Andrade, M. B. Follette, and A. D. Frolov, 2006: The total ozone field separated into meteorological regimes—Part II: Northern Hemisphere mid-latitude total ozone trends. *Atmos. Chem. Phys.*, **6**, 5183–5191, https://doi.org/10.5194/acp-6-5183-2006.

IPCC, 2013: Summary for policymakers. *Climate Change 2013: The Physical Basis*, T. F. Stocker et al., Eds., Cambridge University Press, 3–29.

——, 2014: Summary for policymakers. *Climate Change 2014: Impacts, Adaptation, and Vulnerability*, C. B. Field et al., Eds., Cambridge University Press, 1–32.

Jansen, M., and R. Ferrari, 2012: Macroturbulent equilibration in a thermally forced primitive equation system. *J. Atmos. Sci.*, **69**, 695–713, https://doi.org/10.1175/JAS-D-11-041.1.

Kang, S. M., C. Deser, and L. M. Polvani, 2013: Uncertainty in climate change projections of the Hadley circulation: The role of internal variability. *J. Climate*, **26**, 7541–7554, https://doi.org/10.1175/JCLI-D-12-00788.1.

Levine, X. J., and T. Schneider, 2015: Baroclinic eddies and the extent of the Hadley circulation: An idealized GCM study. *J. Atmos. Sci.*, **72**, 2744–2761, https://doi.org/10.1175/JAS-D-14-0152.1.

Lorenz, D. J., and E. T. DeWeaver, 2007: Tropopause height and zonal wind response to global warming in the IPCC scenario integrations. *J. Geophys. Res.*, **112**, D10119, https://doi.org/10.1029/2006JD008087.

Lu, J., G. A. Vecchi, and T. Reichler, 2007: Expansion of the Hadley cell under global warming. *Geophys. Res. Lett.*, **34**, L06805, https://doi.org/10.1029/2006GL028443.

——, G. Chen, and D. M. W. Frierson, 2008: Response of the zonal mean atmospheric circulation to El Niño versus global warming. *J. Climate*, **21**, 5835–5851, https://doi.org/10.1175/2008JCLI2200.1.

——, C. Deser, and T. Reichler, 2009: Cause of the widening of the tropical belt since 1958. *Geophys. Res. Lett.*, **36**, L03803, https://doi.org/10.1029/2008GL036076.

——, L. Sun, Y. Wu, and G. Chen, 2014: The role of subtropical irreversible PV mixing in the zonal mean circulation response to global warming-like thermal forcing. *J. Climate*, **27**, 2297–2316, https://doi.org/10.1175/JCLI-D-13-00372.1.

Lucas, C., and H. Nguyen, 2015: Regional characteristics of tropical expansion and the role of climate variability. *J. Geophys. Res. Atmos.*, **120**, 6809–6824, https://doi.org/10.1002/2015JD023130.

——, B. Timbal, and H. Nguyen, 2014: The expanding tropics: A critical assessment of the observational and modeling studies. *Wiley Interdiscip. Rev.: Climate Change*, **5**, 89–112, https://doi.org/10.1002/wcc.251.

Mantsis, D. F., S. Sherwood, R. Allen, and L. Shi, 2017: Natural variations of tropical width and recent trends. *Geophys. Res. Lett.*, **44**, 3825–3832, https://doi.org/10.1002/2016GL072097.

Nguyen, H., A. Evans, C. Lucas, I. Smith, and B. Timbal, 2013: The Hadley circulation in reanalyses: Climatology, variability, and change. *J. Climate*, **26**, 3357–3376, https://doi.org/10.1175/JCLI-D-12-00224.1.

Phillips, N. A., 1954: Energy transformations and meridional circulations associated with simple baroclinic waves in a two-level quasi-geostrophic model. *Tellus*, **6**, 273–286, https://doi.org/10.1111/j.2153-3490.1954.tb01123.x.

Polvani, L. M., M. Previdi, and C. Deser, 2011a: Large cancellation, due to ozone recovery, of future Southern Hemisphere atmospheric circulation trends. *Geophys. Res. Lett.*, **38**, L04707, https://doi.org/10.1029/2011GL046712.

——, D. W. Waugh, G. J. P. Correa, and S.-W. Son, 2011b: Stratospheric ozone depletion: The main driver of twentieth-century atmospheric circulation changes in the Southern Hemisphere. *J. Climate*, **24**, 795–812, https://doi.org/10.1175/2010JCLI3772.1.

Quan, X.-W., M. P. Hoerling, J. Perlwitz, H. F. Diaz, and T. Xu, 2014: How fast are the tropics expanding? *J. Climate*, **27**, 1999–2013, https://doi.org/10.1175/JCLI-D-13-00287.1.

Randel, W. J., and I. M. Held, 1991: Phase speed spectra of transient eddy fluxes and critical layer absorption. *J. Atmos. Sci.*, **48**, 688–697, https://doi.org/10.1175/1520-0469(1991)048<0688:PSSOTE>2.0.CO;2.

Santer, B. D., and Coauthors, 2003: Contributions of anthropogenic and natural forcing to recent tropopause height changes. *Science*, **301**, 479–483, https://doi.org/10.1126/science.1084123.

Scheff, J., and D. M. W. Frierson, 2012: Robust future precipitation declines in CMIP5 largely reflect the poleward expansion of model subtropical dry zones. *Geophys. Res. Lett.*, **39**, L18704, https://doi.org/10.1029/2012GL052910.

Seager, R., N. Naik, and G. A. Vecchi, 2010: Thermodynamic and dynamic mechanisms for large-scale changes in the hydrological cycle in response to global warming. *J. Climate*, **23**, 4651–4668, https://doi.org/10.1175/2010JCLI3655.1.

Seidel, D. J., Q. Fu, W. J. Randel, and T. J. Reichler, 2008: Widening of the tropical belt in a changing climate. *Nat. Geosci.*, **1**, 21–24, https://doi.org/10.1038/ngeo.2007.38.

Seviour, W. J. M., S. M. Davis, K. M. Grise, and D. W. Waugh, 2018: Large uncertainty in the relative rates of dynamical and hydrological tropical expansion. *Geophys. Res. Lett.*, **45**, 1106–1113, https://doi.org/10.1002/2017GL076335..

Shaw, T. A., and A. Voigt, 2016: Understanding the links between subtropical and extratropical circulation responses to climate

change using aquaplanet model simulations. *J. Climate*, **29**, 6637–6657, https://doi.org/10.1175/JCLI-D-16-0049.1.

——, and Z. Tan, 2018: Testing latitudinally dependent explanations of the circulation response to increased CO_2 using aquaplanet models. *Geophys. Res. Lett.*, **45**, 9861–9869, https://doi.org/10.1029/2018GL078974.

Smith, K. S., 2007: The geography of linear baroclinic instability in Earth's oceans. *J. Mar. Res.*, **65**, 655–683, https://doi.org/10.1357/002224007783649484

Solomon, A., L. M. Polvani, D. W. Waugh, and S. M. Davis, 2016: Contrasting upper and lower atmospheric metrics of tropical expansion in the Southern Hemisphere. *Geophys. Res. Lett.*, **43**, 10 496–10 503, https://doi.org/10.1002/2016GL070917.

Son, S.-W., N. F. Tandon, L. M. Polvani, and D. W. Waugh, 2009: Ozone hole and Southern Hemisphere climate change. *Geophys. Res. Lett.*, **36**, L15705, https://doi.org/10.1029/2009GL038671.

——, S.-Y. Kim, and S.-K. Min, 2018: Widening of the Hadley cell from Last Glacial Maximum to future climate. *J. Climate*, **31**, 267–281, https://doi.org/10.1175/JCLI-D-17-0328.1.

Staten, P. W., J. J. Rutz, T. Reichler, and J. Lu, 2012: Breaking down the tropospheric circulation response by forcing. *Climate Dyn.*, **39**, 2361–2375, https://doi.org/10.1007/s00382-011-1267-y.

——, T. Reichler, and J. Lu, 2014: The transient circulation response to radiative forcings and sea surface warming. *J. Climate*, **27**, 9323–9336, https://doi.org/10.1175/JCLI-D-14-00035.1.

Tandon, N. F., E. P. Gerber, A. H. Sobel, and L. M. Polvani, 2013: Understanding Hadley cell expansion versus contraction: Insights from simplified models and implications for recent observations. *J. Climate*, **26**, 4304–4321, https://doi.org/10.1175/JCLI-D-12-00598.1.

Taylor, K. E., R. J. Stouffer, and G. A. Meehl, 2012: An overview of CMIP5 and the experiment design. *Bull. Amer. Meteor. Soc.*, **93**, 485–498, https://doi.org/10.1175/BAMS-D-11-00094.1.

Thuburn, J., and G. C. Craig, 1997: GCM tests of theories for the height of the tropopause. *J. Atmos. Sci.*, **54**, 869–882, https://doi.org/10.1175/1520-0469(1997)054<0869:GTOTFT>2.0.CO;2.

——, and ——, 2000: Stratospheric influence on tropopause height: The radiative constraint. *J. Atmos. Sci.*, **57**, 17–28, https://doi.org/10.1175/1520-0469(2000)057<0017:SIOTHT>2.0.CO;2.

Trenberth, K. E., and C. J. Guillemot, 1995: Evaluation of the global atmospheric moisture budget as seen from analyses. *J. Climate*, **8**, 2255–2272, https://doi.org/10.1175/1520-0442(1995)008<2255:EOTGAM>2.0.CO;2.

Vallis, G. K., 2006: *Atmospheric and Oceanic Fluid Dynamics*. Cambridge University Press, 770 pp.

——, P. Zurita-Gotor, C. Cairns, and J. Kidston, 2015: Response of the large-scale structure of the atmosphere to global warming. *Quart. J. Roy. Meteor. Soc.*, **141**, 1479–1501, https://doi.org/10.1002/qj.2456.

Walker, C. C., and T. Schneider, 2006: Eddy influences on Hadley circulations: Simulations with an idealized GCM. *J. Atmos. Sci.*, **63**, 3333–3350, https://doi.org/10.1175/JAS3821.1.

Waugh, D. W., C. I. Garfinkel, and L. M. Polvani, 2015: Drivers of the recent tropical expansion in the Southern Hemisphere: Changing SSTs or ozone depletion? *J. Climate*, **28**, 6581–6586, https://doi.org/10.1175/JCLI-D-15-0138.1.

Wittman, M. A. H., A. J. Charlton, and L. M. Polvani, 2007: The effect of lower stratospheric shear on baroclinic instability. *J. Atmos. Sci.*, **64**, 479–496, https://doi.org/10.1175/JAS3828.1.

Wu, Y., R. Seager, M. Ting, N. Naik, and T. A. Shaw, 2012: Atmospheric circulation response to an instantaneous doubling of carbon dioxide. Part I: Model experiments and transient thermal response in the troposphere. *J. Climate*, **25**, 2862–2879, https://doi.org/10.1175/JCLI-D-11-00284.1.

——, ——, T. A. Shaw, M. Ting, and N. Naik, 2013: Atmospheric circulation response to an instantaneous doubling of carbon dioxide. Part II: Atmospheric transient adjustment and its dynamics. *J. Climate*, **26**, 918–935, https://doi.org/10.1175/JCLI-D-12-00104.1.